行政院國家科學委員會專題研究計畫　成果報告

垂直共振腔雷射橫模之光學圖案形成研究(2/2)

計畫類別： 個別型計畫
計畫編號： NSC92-2112-M-009-036-
執行期間： 92 年 08 月 01 日至 93 年 10 月 31 日
執行單位： 國立交通大學電子物理學系(所)

計畫主持人： 黃凱風

報告類型： 完整報告

處理方式： 本計畫可公開查詢

中　華　民　國 94 年 1 月 14 日

行政院國家科學委員會專題研究計畫成果報告

垂直共振腔雷射橫模之光學圖案形成研究(2/2)

計畫類別：□ 個別型計畫　　□ 整合型計畫

計畫編號：NSC92-2112-M009-036

執行期間：92 年 08 月 01 日至 93 年 10 月 31 日

計畫主持人：黃凱風

本成果報告包括以下應繳交之附件：

□ 赴國外出差或研習心得報告一份

□ 赴大陸地區出差或研習心得報告一份

□ 出席國際學術會議心得報告及發表之論文各一份

□ 國際合作研究計畫國外研究報告書一份

執行單位：國立交通大學電子物理系

中華民國 93 年 12 月 28 日

中文摘要

本計劃最重要的結果是證明在垂直共振腔之高階橫模可應用於同調波波函數圖案之研究。我們量測了方形垂直共振腔雷射之近場與遠場之發光圖案，發現有些與方形二維彈子量子彈子球檯之本徵函數極為接近，而有些則顯示了古典軌跡之圖案，我們將方形之彈子球檯之四個頂角圓滑化後計算其高階之本徵函數，證實圓滑方形結構之對稱性已被破壞，促成 x,y 波函數之混成，形成複雜之圖案，其中有部份顯示出古典之軌跡，與實驗極為吻合，此部份結果已發表於 Phys. Rev. Lett. 89, 224102, (2002)及 PRE.68, 26210,(2003)。

關鍵詞：量子彈子球檯、垂直共振腔面射型雷射、光學圖案

Observation of theWave Function of a Quantum Billiard from the Transverse Patterns of Vertical Cavity Surface Emitting Lasers

K. F. Huang, Y. F. Chen,* and H.C. Lai

Department of Electrophysics, National Chiao Tung University, Hsinchu, Taiwan, Republic of China

Y. P. Lan

Institute of Electro-Optical Engineering, National Chiao Tung University, Hsinchu, Taiwan, Republic of China

(Received 26 April 2002; published 11 November 2002)

We demonstrate experimentally that the near-field and far-field transverse patterns of a large aperture vertical cavity surface emitting laser (VCSEL) can be successfully interpreted as a two-dimensional (2D) billiard system. It is found that the near-field and far-field transverse patterns of a large aperture VCSEL evidently represent the coordinate-space and momentum-space wave functions of a 2D quantum billiard, respectively. The result of this paper suggests that large aperture VCSELs are potentially appropriate physical systems for the wave-function study in quantum problems.

DOI: 10.1103/PhysRevLett.89.224102 PACS numbers: 05.45.Mt, 42.55.Sa, 42.60.Jf

Rules of selection for spontaneous coherent states in mesoscopic systems: Using the microcavity laser as an analog study

Y. F. Chen,* K. F. Huang, and H. C. Lai

Department of Electrophysics, National Chiao Tung University, 1001 TA Hsueh Road, Hsinchu, Taiwan 30050

Y. P. Lan

Institute of Electro-Optical Engineering, National Chiao Tung University, Hsinchu, Taiwan

~Received 2 April 2003; published 19 August 2003!

The selection rules for spontaneous coherent waves in mesoscopic systems are experimentally studied using the transverse patterns of a microcavity laser and theoretically analyzed using the theory of SU~2! coherent states. Comparison of the experimental results with the theoretical analyses reveals that an amplitude factor *A* should be included in the representation of the partially coherent states. The determination of the amplitude factor *A* is found to be associated with the constraint of minimum energy uncertainty.

DOI: 10.1103/PhysRevE.68.026210 PACS number~s!: 05.45.2a, 03.65.Ge, 42.55.Sa, 73.23.Ad

Observation of the Wave Function of a Quantum Billiard from the Transverse Patterns of Vertical Cavity Surface Emitting Lasers

K. F. Huang, Y. F. Chen,* and H. C. Lai
Department of Electrophysics, National Chiao Tung University, Hsinchu, Taiwan, Republic of China

Y. P. Lan
Institute of Electro-Optical Engineering, National Chiao Tung University, Hsinchu, Taiwan, Republic of China
(Received 26 April 2002; published 11 November 2002)

We demonstrate experimentally that the near-field and far-field transverse patterns of a large aperture vertical cavity surface emitting laser (VCSEL) can be successfully interpreted as a two-dimensional (2D) billiard system. It is found that the near-field and far-field transverse patterns of a large aperture VCSEL evidently represent the coordinate-space and momentum-space wave functions of a 2D quantum billiard, respectively. The result of this paper suggests that large aperture VCSELs are potentially appropriate physical systems for the wave-function study in quantum problems.

DOI: 10.1103/PhysRevLett.89.224102 PACS numbers: 05.45.Mt, 42.55.Sa, 42.60.Jf

Vertical cavity surface emitting lasers (VCSELs) have become of considerable interest for short-range data communications and sensor applications [1]. Of scientific interest, VCSELs inherently emit in single-longitudinal mode due to their extremely short cavity length, but large aperture devices can exhibit a complex transverse mode structure. The transverse mode pattern and the polarization instabilities in VCSELs have been the main interests in the past few years [2–7]. Hegarty *et al.* [8] reported interesting transverse mode patterns from oxide-confined square-shaped VCSELs with larger aperture. Their experimental results revealed that a wave incident upon the current-guiding oxide boundary would undergo total internal reflection because of large index discontinuities between the oxide layer and the surrounding semiconductor material. Namely, VCSELs can be considered as a planar waveguide with a dominant wave vector along the vertical direction. Because of the analogy between the Schrodinger and Helmholtz equations [9], it is essentially feasible to use the oxide-confined VCSEL cavities, such as microwave cavities [10,11], to represent quantum mechanical potential wells. In this case, the transverse patterns can reveal the probability density of the corresponding wave functions to the two-dimensional quantum billiards. However, such a correspondence has not been established as yet because the thermal effects usually result in a complex refraction-index distribution to distort the VCSEL planoplanar resonators [6].

In this Letter, we experimentally demonstrate that, when the thermal effects are reduced by cooling the device at the temperature below 10 °C, the near-field and far-field transverse patterns of a large aperture VCSEL evidently represent the coordinate-space and momentum-space wave functions of a 2D quantum billiard, respectively. The satisfactory correspondence implies that VCSELs are appropriate devices for the study of the behavior of the wave functions in quantum billiard problems. Since VCSELs, in general, can be fabricated for any two-dimensional shape, this versatility makes these devices extremely flexible to explore a great deal of interesting physics.

In this investigation, we fabricate square-shaped VCSELs with large aperture and measure near-field and far-field patterns of the transverse mode. The size of the oxide aperture is $40 \times 40\ \mu m^2$. The device structure of these oxide-confined VCSELs and the methods used to measure the far-field and near-field patterns are similar to those described by Ref. [8]. Experimental results show that the transverse patterns of VCSELs can be certainly divided into two regimes of low-divergence and high-divergence emissions. Hereafter, we will concentrate on the high-divergence emission, which appears only at reduced temperature and near threshold operation. It is expected the thermal-lensing effect will switch the device into the low-divergence regime because the joule heating induces a temperature rise across the device cross section. Typically, high-divergence patterns are very symmetric and those of low divergence are more irregular. Therefore it is easy to differentiate the regimes in which the lasers are being operated.

We first controlled the device at the temperature of 10 °C. As shown in Fig. 1, the near-field pattern of the device was found to be a bouncing-ball scar that is similar to the result of Ref. [8], except that the order is higher. It can be seen that the observed bouncing-ball scar is not perfectly periodic but contains dislocations to show some wavy structure. Even so, the laser beam was measured to be linearly polarized. As the device was cooled at the temperature around 0 °C, the near-field pattern changed dramatically, as shown in Fig. 2. It can be seen that the near-field intensity apparently was highly concentrated along the trajectory of a diamond-shaped classical orbit. Although this diamond "scar" has been discussed extensively in the wave functions of ballistic quantum dots

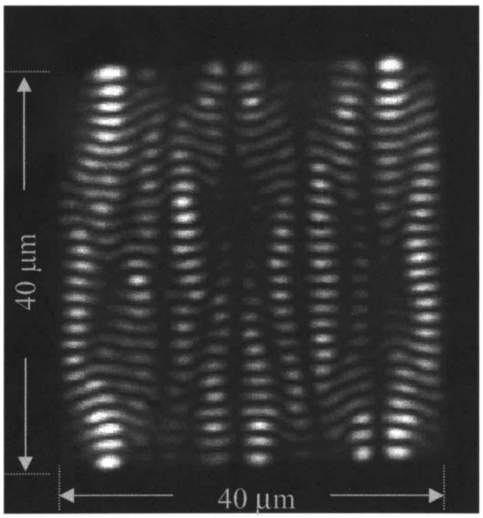

FIG. 1. The experimental result for the near-field pattern of the VCSEL device near the lasing threshold. The device was operated at the temperature 10 °C.

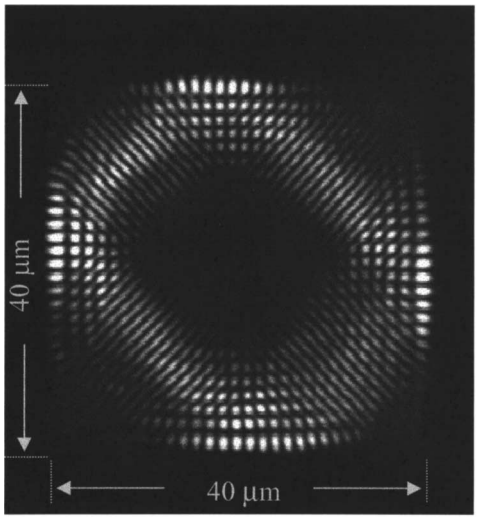

FIG. 2. The experimental result for the near-field pattern of the VCSEL device near the lasing threshold. The device was operated at the temperature 0 °C

[12–14], it is the first time to observe this interesting pattern from a laser transverse pattern. The specific wave scars confirm the fact that the oxide-confined VCSELs can be considered as a planar waveguide.

In order to understand the observed transverse patterns, it is helpful to simplify the VCSEL structure first. We consider the large aperture VCSEL to be a very narrow square-shaped three-dimensional resonator with embedded gain material. The two distributed feedback reflectors (DBR) were separated by nearly one wavelength and the square-shaped oxide aperture defined the lateral billiard boundary. The wave vectors can be decomposed into k_z and k_t, where k_z is the wave-vector component along the direction of vertical emission and k_t is the transverse wave-vector component. Since the vertical dimension is designed to be nearly one wavelength, k_z is the dominating component in the emission wave vector. The lateral boundary has a dimension of $40 \times 40\ \mu\text{m}^2$; consequently, the transverse k_t is much smaller than k_z. The lateral oxide boundary can be considered as rigid walls with infinite potentials since the photons will experience total reflection at the lateral oxide walls due to a large k_z component and a relatively small transverse component k_t. Furthermore, since the mirrors in VCSELs are DBRs, they can be considered as plane mirrors with no curvature. The photons can be treated as particles confined in a boundary with infinite potential and zero potential inside the square. Vertical emission in the z direction can be considered to be the coupling of the resonance fields inside the cavity to the outside medium through the top DBR. Therefore, the phasor amplitude of the emission field distribution $E(x, y, z)$ is conveniently given by $E(x, y, z) = \psi(x, y)e^{-jk_z z}$. After separating the z component in the wave equation, we are left with a two-dimensional Helmholtz equation: $(\nabla_t^2 + k_t^2)\psi(x, y) = 0$. Here, ∇_t^2 means the Laplacian operator operating on the coordinates in the transverse plane and $\psi(x, y)$ is a scalar wave function that describes the transverse profile of the laser. The solutions to the Helmholtz equation with total internal reflection boundaries are equivalent to the solutions of the 2D Schrodinger equation with hard wall boundaries [$\psi(x, y) = 0$ at the boundary] of the same geometry. This analogy has been exploited most successfully in microwave cavities and scarred eigenfunctions of a chaotic billiard have been demonstrated [10,11]. The wave functions for the 2D quantum billiards are also important understanding the behavior of mesoscopic structures, and will be crucial for the design of nanoscale electronic devices [12–14].

It is well known that the solution to a perfect square billiard can be obtained by separation of variables. However, this subtle solution definitely cannot account for the present observed pattern. It is self-evident that the perfect square billiard is quite rare in most of the real physical problems. In real VCSEL devices, the square aperture is fabricated first by etching a square mesa and then oxidizes the AlAs layer to form the oxide boundary. Process induced deformation is unavoidable, and therefore a perfect square billiard is not appropriate for the simulation. In order to simulate the square billiard formed by the oxide aperture, we modify the square by rounding off the corners. With the rounded off square boundary, the Helmholtz equation can no longer be solved by the method of separation of variables. We use a numerical method called expansion method [15] to solve the equation. Because of symmetry breaking, the eigenfunctions obtained are much more interesting than those of the perfect square billiard. For low order solutions, the patterns are similar to those of the perfect square billiard. However, the higher order eigenfunctions are drastically different in structure and very rich patterns appear. It is of surprising interest that some of the solutions display the

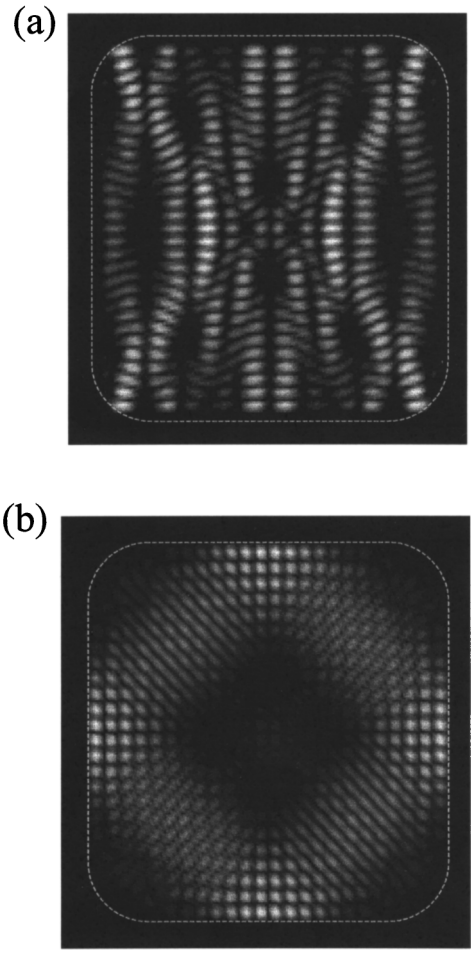

FIG. 3. The calculated wave functions of the square billiards modified by rounding off the corners. (a) and (b) are similar to the observed near-field patterns in Figs. 1 and 2, respectively. The dashed lines indicate the boundary of the simulation.

distorted bouncing-ball and diamond-shaped scars similar to the experimental results. Figure 3 shows two of the calculated eigenfunctions that are similar to the observed near-field patterns in Figs. 1 and 2. Note that the present modified square billiards always have the high-order eigenfunctions demonstrating the distorted bouncing-ball and diamond-shaped scars, almost irrelevant to the degree of how much the corners are rounded off.

It is worthwhile to mention that Nöckel and Stone [16] have designed stadium-shaped microcavity lasers and demonstrated high power directional emission in the midinfrared wavelength based on some chaotic two-dimensional billiard dynamics. However, due to the geometrical structure of the laser, only edge emission was allowed in these deformed microdisk lasers. Therefore, a comparison between the experimentally determined far-field pattern and simulation was limited for only one dimension. The near-field pattern was not measured because high-resolution midinfrared detection was not possible.

The optical far-field intensity essentially is the spatial 2D Fourier transform (FT) of the near-field pattern, while the FT of the coordinate-space wave function corresponds to the momentum-space representation in the quantum mechanics. Recently, Delande and Sornette [17] have calculated the acoustic radiation from a stadium-shaped membrane by applying FT to the eigenfunctions. Similar calculations focusing on the momentum representation of the wave functions were also reported by Bäcker and Schubert [18]. Both theoretical papers suggested that momentum distribution of a two-dimensional quantum billiard is actually experimentally observable and such information can provide a more comprehensive understanding to the billiard system. Therefore, it is consequentially meaningful to measure the far-field pattern for the VCSEL devices. Figure 4 shows the experimental observation of the far-field pattern corresponding to the diamond-shaped wave function in Fig. 2. It can be clearly seen that the far-field pattern exhibited some strong intensity lotus flower structure at the corners of the square and some weak stripes connecting the lotus structure. This far-field pattern is consistent with the near-field

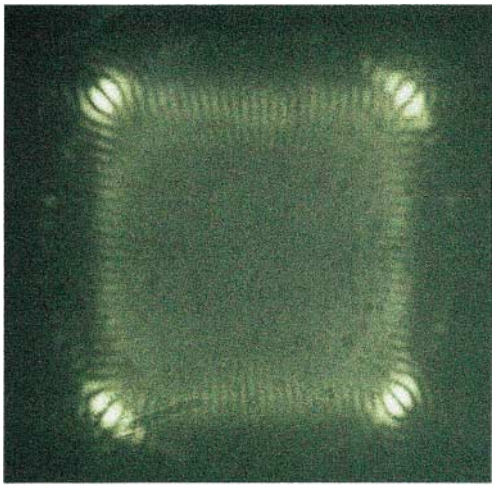

FIG. 4 (color). The experimental result for the far-field pattern corresponding to the near-field pattern in Fig. 2.

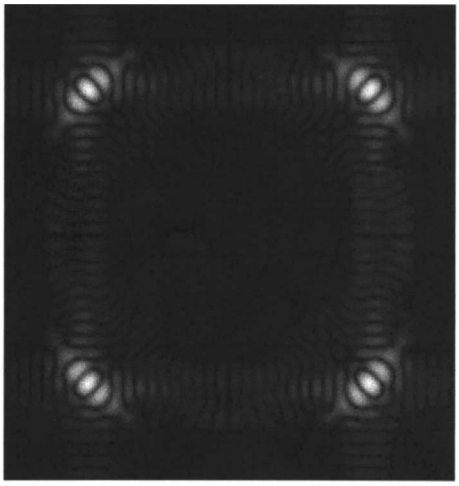

FIG. 5. The calculated momentum-space wave function corresponding to the coordinate-space wave function in Fig. 3(b).

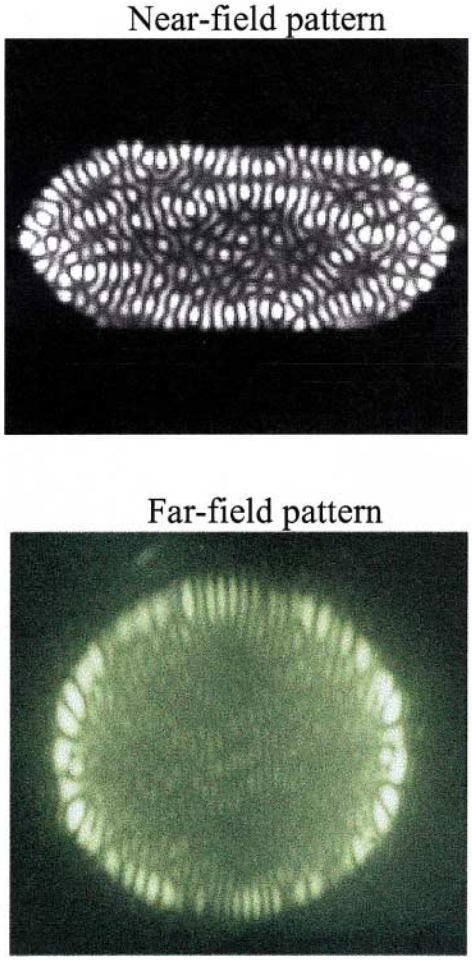

FIG. 6 (color). Experimental results of the near-field and far-field patterns for the VCSEL device with a stadium-shaped boundary.

diamond-shaped scar that apparently was concentrated along the trajectory traced by a particle bouncing off the neighboring walls of the square. Figure 5 shows the momentum-space wave function of the theoretical diamond-shaped scar shown in Fig. 3. The good agreement between experimental results and theoretical calculations confirms our physical analysis and validates the present theoretical model.

Finally, it is worthwhile to clarify that the present interpretation is based on the assumption that the influence of carrier dynamics on the transverse pattern near threshold is negligible. To further justify this assumption, we fabricated the devices with a shape of Bunimovich stadium boundary and measured the near-field and far-field intensities. As shown in Fig. 6, the near-field intensity displays a scarred pattern and the far-field intensity resembles the calculated results of Refs. [17,18] in appearance. The boundary-shape dependence of the VCSEL patterns confirms the present interpretation.

In conclusion, we have observed unique near- and far-field transverse patterns in large aperture VCSELs. A two-dimensional quantum billiard model is utilized to explain the experiments. It turns out the square billiard with minor modification is adequate to simulate the real device. Rounding off the corners certainly breaks the symmetry and introduces coupling of the two originally independent variables. This symmetry breaking makes the solution of the high-order eigenfunctions much more interesting as they display highly graphical patterns. The observed near-field pattern in the transverse mode apparently can be interpreted as from these solutions. Furthermore, the corresponding far-field patterns can also be explained by the momentum-space wave functions in the billiard. The result of this paper also suggests that large aperture VCSELs are potentially appropriate physical systems for the quantum chaos study.

The authors gratefully acknowledge various VCSEL devices from TrueLight Corporation. The authors also thank the National Science Council for their financial support of this research under Contract No. NSC-91-2112-M-009-030.

*Corresponding author.
Electronic address: yfchen@cc.nctu.edu.tw

[1] W.W. Chow, K.D. Choquette, M. Hagerot-Crowford, K.L. Lear, and G.R. Hadley, IEEE J. Quantum Electron. **33**, 1810 (1997).
[2] M. San Miguel, Q. Feng, and J.V. Molony, Phys. Rev. A **52**, 1728 (1995).
[3] M.P. van Exter, M.B. Willemsen, and J.P. Woerdman, Phys. Rev. A **58**, 4191 (1998).
[4] S. Balle, E. Tolkachova, M. San Miguel, J.R. Tredicce, J. Martin-Regalado, and A. Gahl, Opt. Lett. **24**, 1121 (1999).
[5] M. Brambilla, L.A. Lugiato, F. Prati, L. Spinell, and W.J. Firth, Phys. Rev. Lett. **79**, 2042 (1997).
[6] T. Ackeman, S. Barland, M. Cara, S. Balle, J.R. Tredicce, R. Jäger, M. Grabherr, M. Miller, and K.J. Ebeling, J. Opt. B **2**, 406 (2000).
[7] C. Degen, I. Fischer, and W. Elsäßer, Opt. Ex. **5**, 38 (1999).
[8] S.P. Hegarty, G. Huyet, J.G. McInerney, and K.D. Choquette, Phys. Rev. Lett. **82**, 1434 (1999).
[9] J.J. Hupert and G. Ott, Am. J. Phys. **34**, 260 (1966).
[10] S. Sridhar, Phys. Rev. Lett. **67**, 785 (1991).
[11] J. Stein and H.J. Stöckmann, Phys. Rev. Lett. **68**, 2867 (1992).
[12] R. Akis, D.K. Ferry, and J.P. Bird, Phys. Rev. Lett. **79**, 123 (1997).
[13] R. Akis, D.K. Ferry, J.P. bird, and D. Vasileska, Phys. Rev. B **60**, 2680 (1999).
[14] Y.H. Kim, M. Barth, H.J. Stöckmann, and J.P. Bird, Phys. Rev. B **65**, 165317 (2002).
[15] D.L. Kaufman, I. Kosztin, and K. Schulten, Am. J. Phys. **67**, 133 (1999).
[16] J.U. Nöckel and A.D. Stone, Nature (London) **385**, 45 (1997).
[17] D. Delande and D. Sornette, J. Acoust. Soc. Am. **101**, 1793 (1997).
[18] A. Bäcker and R. Schubert, J. Phys. A **32**, 4795 (1999).

Rules of selection for spontaneous coherent states in mesoscopic systems: Using the microcavity laser as an analog study

Y. F. Chen,* K. F. Huang, and H. C. Lai
Department of Electrophysics, National Chiao Tung University, 1001 TA Hsueh Road, Hsinchu, Taiwan 30050

Y. P. Lan
Institute of Electro-Optical Engineering, National Chiao Tung University, Hsinchu, Taiwan
(Received 2 April 2003; published 19 August 2003)

The selection rules for spontaneous coherent waves in mesoscopic systems are experimentally studied using the transverse patterns of a microcavity laser and theoretically analyzed using the theory of SU(2) coherent states. Comparison of the experimental results with the theoretical analyses reveals that an amplitude factor A should be included in the representation of the partially coherent states. The determination of the amplitude factor A is found to be associated with the constraint of minimum energy uncertainty.

DOI: 10.1103/PhysRevE.68.026210 PACS number(s): 05.45.−a, 03.65.Ge, 42.55.Sa, 73.23.Ad

Recently, the progress in modern semiconductor technology has made it possible to design nanostructure devices with quantum ballistic properties [1]. The results of recent studies of open square quantum dots show that the striking phenomena of conductance fluctuations are associated with wave patterns localized on classical periodic orbits [2–4]. The general principles of pattern formation indicate that small disturbances can cause the real system to select some states from the range available to the idealized perfect system [5,6]. Although there are mathematically many possible selections, the experimental results reveal that the wave patterns associated with classical periodic orbits are often the persistent states in mesoscopic systems [7–9]. Therefore, to establish the relation between the quantum wave functions and the classical periodic orbits is a crucial phase in investigating the quantum phenomena in mesoscopic systems [10,11]. In this work, we experimentally and theoretically study the selection rules for the spontaneous coherent states associated with the classical periodic orbits in mesoscopic systems.

In recent years, microwave cavities have been used to perform analog studies of transport in open quantum dots [7–9]. More recently, we demonstrated that the transverse patterns of oxide-confined vertical-cavity surface-emitting lasers (VCSEL's) reveal the probability density of the wave functions corresponding to two-dimensional (2D) quantum billiards [12]. Here we use square-shaped VCSEL's with 40 μm oxide aperture to investigate the variations of the transverse pattern with the heat sink temperature. The emission wavelength near the lasing threshold is normally close to the peak gain wavelength, which shifts with temperature (0.2–0.3 nm/K) at a faster rate than does the VCSEL cavity resonance. The transverse-mode spacing can be derived as $\Delta\lambda \approx \lambda^3/(4a^2)$, where $\lambda \approx 780$ nm is the fundamental wavelength and a is the length of the square boundary. Since the transverse-mode spacing is around $\Delta\lambda \approx 0.07$ nm, the transverse patterns of VCSEL's can be easily detuned by controlling the heat sink temperature. Although an ideal 2D square billiard has many possible eigenstates, only a few stationary states are observed in experimental transverse patterns. As shown in Fig. 1, only three types of transverse pattern are usually observed by detuning the temperature from 280 to 240 K. Similar to the quantum flows in open square quantum dots [2–4], the observed transverse patterns of square-shaped VCSEL's are concentrated along classical periodic orbits instead of being regular eigenstates of the perfect square billiard. The present result supports the idea that the properties of the wave functions in mesoscopic structures can be analogously studied by designing optical structures with similar or identical functional forms [13]. Recently, Doya *et al.* [14] introduced the paraxial approximation to establish an analogy between light propagation along a multimode fiber and quantum-confined systems. It is believed that these analogies will continue to be exploited for understanding the physics of mesoscopic systems.

Previously, we analytically constructed the wave functions related to the primitive periodic orbit (p,q,ϕ) in a 2D square billiard by using the representation of SU(2) coherent states, where p and q are two positive integers describing the number of collisions with the horizontal and vertical walls, and the phase factor ϕ $(-\pi \leqslant \phi \leqslant \pi)$ that is related to the wall positions of specular reflection points [15]. As in the Schwinger representation of the SU(2) algebra, the wave

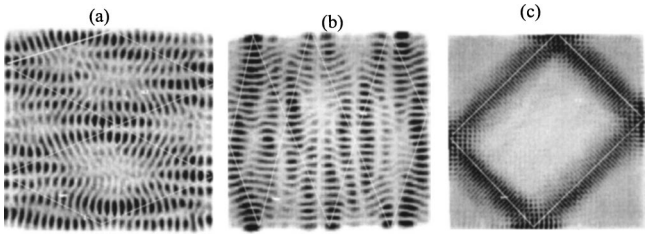

FIG. 1. The experimental near-field patterns of the VCSEL device near the lasing threshold at temperatures around (a) 270–280, (b) 260–270, and (c) 240–260 K. The white lines superimposed on top of the wave patterns indicate the related classical periodic orbits.

*Author to whom correspondence should be addressed. FAX: 886-35 729134. Electronic address: yfchen@cc.nctu.edu.tw

function associated with high-order periodic orbits (p,q,ϕ) is analytically expressed as [15]

$$\Psi_N^{p,q}(x,y;\tau)=\frac{(2/a)}{(1+|\tau|^2)^{N/2}}\sum_{K=0}^{N}\sqrt{C_K^N}\tau^K \times\sin\left[p(K+1)\frac{\pi x}{a}\right]\sin\left[q(N-K+1)\frac{\pi y}{a}\right], \tag{1}$$

where a is the length of the square boundary, N represents the order of the coherent state, K is associated with the order of the eigenstates, C_K^N is the binomial coefficient, and the parameter τ is related to the phase factor ϕ by $\tau=\exp(i\phi)$. The relationship between the parameter ϕ and the periodic orbits can be understood by using the identity $\sin z=(e^{iz}-e^{-iz})/2i$ to rewrite Eq. (1) and applying the property of the *Dirichlet kernel*. A detailed discussion can be found in Ref. [15]. Using Eq. (1) and $|\tau|^2=1$, the ratio of the average speeds along the x and y axes in the classical limit $(N\to\infty)$ is found to be p/q. The result of $\sqrt{\langle\nu_x^2\rangle/\langle\nu_y^2\rangle}=p/q$ is consistent with the requirement of classical periodic orbits. On the other hand, $\Delta H/\langle H\rangle$ is inversely proportional to N, where $\langle H\rangle$ is the expectation value of the Hamiltonian and ΔH is the dispersion in energy obtained by computing $\sqrt{\langle H^2\rangle-\langle H\rangle^2}$. Therefore, $\Delta H/\langle H\rangle\to 0$ as $N\to\infty$. This asymptotic property indicates that the coherent states in Eq. (1) are stationary states in the classical limit. However, the coherent state in Eq. (1) for mesoscopic systems, i.e., N is finite, is generally not a stationary state for the Hamiltonian of a perfect square billiard because the eigenstate components are not degenerate.

For mesoscopic systems, the experimental phenomena reveal that the parameter τ should be generalized as $A\exp(i\phi)$, where the amplitude factor A is a positive real value. With $\tau=A\exp(i\phi)$, Eq. (1) becomes

$$\Psi_N^{p,q}(x,y;A,\phi)=\frac{(2/a)}{(1+A^2)^{N/2}}\sum_{K=0}^{N}\sqrt{C_K^N}A^K e^{iK\phi} \times\sin\left[p(K+1)\frac{\pi x}{a}\right] \times\sin\left[q(N-K+1)\frac{\pi y}{a}\right]. \tag{2}$$

It can be found that the coherent states in Eq. (2) have the asymptotic behavior

$$\Psi_N^{p,q}(x,y;A,\phi) \sim\begin{cases}(2/a)\sin(p\pi x/a)\sin[q(N+1)\pi y/a] & (A\to 0),\\ (2/a)\sin[p(N+1)\pi x/a]\sin(q\pi y/a) & (A\to\infty).\end{cases}$$

Nevertheless, the amplitude factor A in the range of 0.1–10 has a great deal to do with the fine structure of wave patterns. It will be demonstrated later that the determination of the amplitude factor A plays an important role in comparing the theoretical calculations with the experimental results. Hereafter the amplitude factor A is considered in the range of 0.1–10 unless otherwise specified.

Comparison of the experimental results with the theoretical analyses reveals that the coherent state in Eq. (2) should be modified to be a partially coherent state that includes 3–7 nearly degenerate eigenstates. In fact, only a few nearly degenerate eigenstates are already sufficient to localize wave patterns on high-order periodic orbits [15]. Moreover, the coherent state in Eq. (2) represents a traveling-wave property. To make a comparison with experimental results, the standing-wave representations can be obtained by replacing the factor $e^{iK\phi}$ by $\sin(K\phi)$ or $\cos(K\phi)$. Accordingly, the partially coherent state can be defined as

$$\Psi_{N,M}^{p,q}(x,y;A,\phi)=\frac{(2/a)}{\left[\sum_{K=K_0-J}^{K_0+J}C_K^N A^{2K}\sin^2(K\phi)\right]^{1/2}} \times\sum_{K=K_0-J}^{K_0+J}\sqrt{C_K^N}A^K\sin(K\phi) \times\sin\left[p(K+1)\frac{\pi x}{a}\right] \times\sin\left[q(N-K+1)\frac{\pi y}{a}\right], \tag{3}$$

where $K_0=[N(A^2/1+A^2)]$, the symbol $[\nu]$ denotes the largest integer $\leqslant\nu$, and the index $M=2J+1$ represents the number of eigenstates used in the state $\Psi_{N,M}^{p,q}(x,y;A,\phi)$. The number of eigenstates M is somewhat restricted because $\Delta H/\langle H\rangle$ is generally proportional to the index M for a given order N. In most cases, experimental results reveal that $3\leqslant M\leqslant 7$. Note that the coefficient $C_K^N A^{2K}$ is associated with the relative probability amplitude of the eigenstate $(2/a)\sin[p(K+1)(\pi x/a)]\sin[q(N-K+1)(\pi y/a)]$ and its value is maximum for $K=K_0$. To be brief, the partially coherent state is a superposition of a few eigenstates next to the eigenstates of maximum probability in the standard SU(2) representation.

As mentioned earlier, the partially coherent states in Eq. (3) are also not stationary states for a perfect square billiard. Nevertheless, the spontaneous symmetry breaking or weak perturbation may cause the partially coherent state to be a stationary state. Since the amplitude factor A has much to do with the fine structure of the wave pattern, it is much more informative to comprehend the A dependence of the energy uncertainty $\Delta H/\langle H\rangle$ for the partially coherent state $\Psi_{N,M}^{p,q}(x,y;A,\phi)$. Figure 2 shows the A dependence of the energy uncertainty $\Delta H/\langle H\rangle$ and several related patterns for the partially coherent state $\Psi_{30,5}^{1,2}(x,y;A,0.47\pi)$. The value of the phase ϕ is determined by the best fit for experimental results. It can be seen that the partially coherent state $\Psi_{30,5}^{1,2}(x,y;A,0.47\pi)$ has a minimum energy uncertainty around $A=2.15$. More importantly, the wave pattern with the minimum energy uncertainty agrees very well with the experimental result depicted in Fig. 1(a).

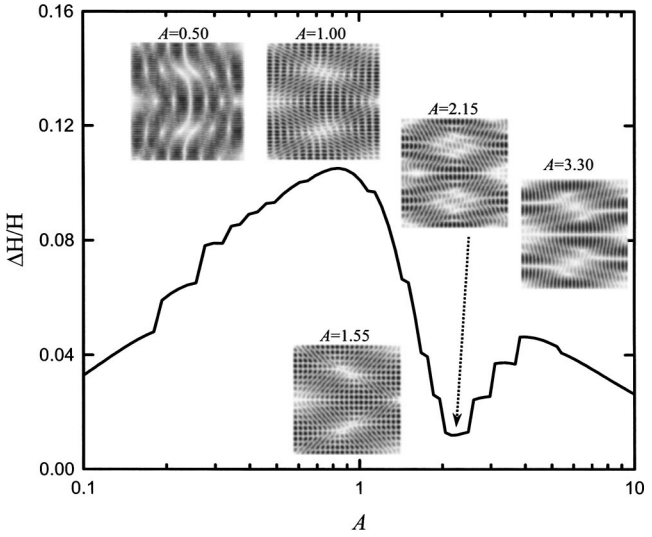

FIG. 2. The calculated results of the A dependence of the energy uncertainty $\Delta H/\langle H\rangle$ for the partially coherent state $\Psi^{1,2}_{30,5}(x,y;A,0.47\pi)$. Several calculated patterns for different values of A are shown in the insets; the calculated pattern with minimum $\Delta H/\langle H\rangle$ corresponds to the experimental result shown in Fig. 1(a).

Similar plots for partially coherent states $\Psi^{3,1}_{29,3}(x,y;A,0.55\pi)$ and $\Psi^{1,1}_{80,7}(x,y;A,0.45\pi)$ are shown in Figs. 3 and 4, respectively. Here again the wave patterns with minimum $\Delta H/\langle H\rangle$ are in good agreement with experimental results shown in Figs. 1(b) and 1(c). Therefore, it can be concluded that the partially coherent states with minimum energy uncertainty in perfect systems usually become the eigenstates in those systems with small disturbances or tiny symmetry breaking. In other words, the wave function obtained as a linear superposition of a few nearly degenerate eigenstates can provide a more physical description of a phenomenon than the true eigenstates in real mesoscopic systems. Even so, the pump profile should be essentially uniform to guarantee that the partially coherent state is the correct criterion for a VCSEL laser just above threshold.

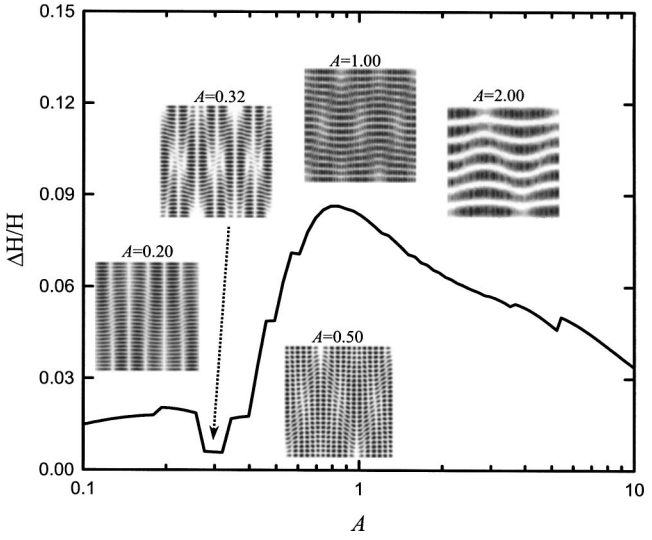

FIG. 3. Similar to Fig. 2 for $\Psi^{3,1}_{29,3}(x,y;A,0.55\pi)$; the calculated pattern with minimum $\Delta H/\langle H\rangle$ corresponds to the experimental result shown in Fig. 1(b).

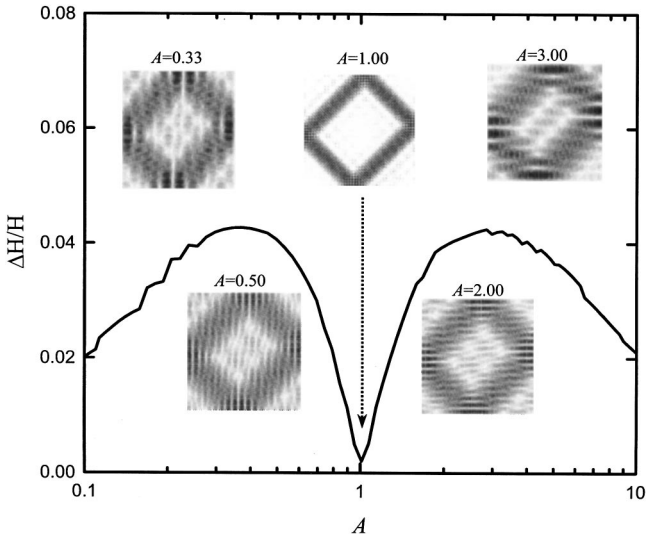

FIG. 4. Similar to Fig. 2 for $\Psi^{1,1}_{80,7}(x,y;A,0.45\pi)$; the calculated pattern with minimum $\Delta H/\langle H\rangle$ corresponds to the experimental result shown in Fig. 1(c).

Since the partially coherent states also often appear in weakly perturbed 2D square billiards [5,6] and in the ballistic quantum dot at resonance [2–4], we use the present model to analyze the resonant-energy states of an open square quantum dot. It can be seen that the theoretical result $\Psi^{1,2}_{40,5}(x,y;2.15,0.5\pi)$ shown in Fig. 5(b) agrees quite well with the representative data of Ref. [4] shown in Fig. 5(a).

Although the specific origin of spontaneous symmetry breaking is still an open question, it is of great value to make a comparison between spontaneous and deliberate symmetry breakings with the present devices. We have fabricated VCSEL's with a ripple boundary to experimentally study the influence of the degree of symmetry breaking. With a considerable ripple boundary, the experimental patterns are always found to be ergodic. Intriguingly, the coexistence of localized and ergodic states is observed in a device with a moderate ripple boundary, as shown in Fig. 6. Even so, the

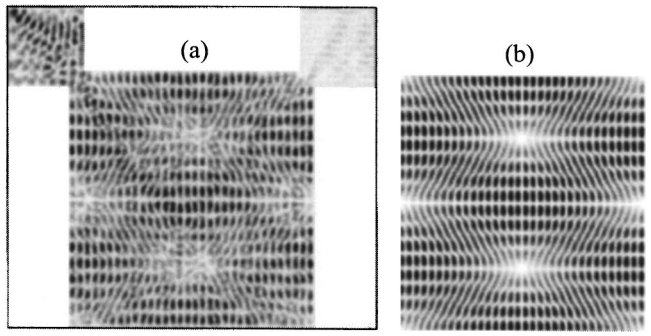

FIG. 5. Comparison of the resonant-energy states of an open square quantum dot with the theoretical result $\Psi^{1,2}_{40,5}(x,y;2.15,0.5\pi)$: (a) resonant pattern from Ref. [4]; (b) the calculated pattern.

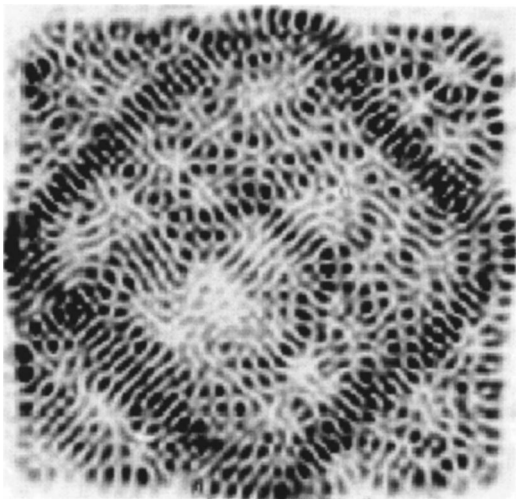

FIG. 6. The experimental near-field pattern of the VCSEL device with a moderate ripple boundary.

partially coherent states localized on the classical orbits are generic and structurally stable in square-shaped VCSEL's without any deliberate symmetry breaking. In brief, a spontaneous symmetry breaking is necessary to lead to the localized states in a square billiard; however, a nonspontaneous one may drive the states into the ergodic regime. Although the quantitative analysis is difficult at the moment, the transition from the localized to ergodic regime is basically consistent with the theoretical analysis of a ripple billiard [5]. A similar transition is also found in the theoretical study of a circular billiard with rough boundaries [16]. It has been numerically shown that the smaller the roughness, the wider the localized regime, even though the state order entering the localized regime becomes higher. In opposition, if the roughness is large to a certain extent, the localized regime is significantly narrowed and the wave function may become utterly ergodic.

Finally, it is worthwhile to connect the present experimental results with similar phenomena discussed in other systems. As a rule, any system is always coupled to some environment and therefore it is never really closed. Nazmitdinov *et al.* [8] have used the effective Hamiltonian to calculate wave functions and coupling coefficients to the environment for the Bunimovich stadium with two attached leads. Their study shows that two types of wave function exist in the open quantum billiard. One type is the short-lived special states that are localized around the classical paths; the other is the long-lived trapped states that are distributed over the whole cavity. Both types of wave function have been observed in the present experiment. Even so, the selection of the states in open systems strongly depends on the condition of the coupling to the environment, as already mentioned in Ref. [8]. In VCSEL devices, the coupling to the environment mostly arises from the vertical mirror. In open quantum dots, however, the coupling is usually through the attached leads. Therefore, the influence of the coupling strength on the localization of the wave functions would be somewhat dissimilar for different open systems.

In summary, the transverse pattern of a microcavity laser has been used to experimentally study the selection rules of spontaneous coherent waves in mesoscopic systems. With the theory of SU(2) coherent states, the spontaneous transverse pattern of a microcavity laser can be described very well. The constraint of minimum energy uncertainty is found to play an important role in selecting the spontaneous coherent states in mesoscopic systems. Moreover, the selection rules are confirmed to be applicable to the resonant-energy states of open square quantum dots.

[1] K. Richter, D. Ullmo, and R. A. Jalabert, Phys. Rep. **276**, 1 (1996).
[2] R. Akis and D. K. Ferry, Phys. Rev. B **59**, 7529 (1999).
[3] I. V. Zozoulenko and K. F. Berggren, Phys. Rev. B **56**, 6931 (1997).
[4] I. V. Zozoulenko, R. Schuster, K. F. Berggren, and K. Ensslin, Phys. Rev. B **55**, R10209 (1997).
[5] W. Li, L. E. Reichl, and B. Wu, Phys. Rev. E **65**, 056220 (2002).
[6] R. Narevich, R. E. Prange, and O. Zaitsev, Phys. Rev. E **62**, 2046 (2000).
[7] Y. H. Kim, M. Barth, H. J. Stöckmann, and J. P. Bird, Phys. Rev. B **65**, 165317 (2002).
[8] R. G. Nazmitdinov, K. N. Pichugin, I. Rotter, and P. Šeba, Phys. Rev. B **66**, 085322 (2002).
[9] T. Blomquist, H. Schanze, I. V. Zozoulenko, and H. J. Stöckmann, Phys. Rev. E **66**, 026217 (2002).
[10] F. von Oppen, Phys. Rev. B **50**, 17 151 (1994).
[11] D. Ullmo, K. Ritcher, and R. A. Jalabert, Phys. Rev. Lett. **74**, 383 (1995).
[12] K. F. Huang, Y. F. Chen, H. C. Lai, and Y. P. Lan, Phys. Rev. Lett. **89**, 224102 (2002).
[13] D. Dragoman and M. Dragoman, Prog. Quantum Electron. **23**, 131 (1999).
[14] V. Doya, O. Legrand, F. Mortessagne, and C. Miniatura, Phys. Rev. Lett. **88**, 014102 (2002).
[15] Y. F. Chen, K. F. Huang, and Y. P. Lan, Phys. Rev. E **66**, 066210 (2002).
[16] K. M. Frahm and D. L. Shepelyansky, Phys. Rev. Lett. **78**, 1440 (1997).